PCCP

PAPER

View Article Online
View Journal | View Issue

Cite this: *Phys. Chem. Chem. Phys.*, 2021, **23**, 19386

Microelectrode-based transient amperometry of O_2 adsorption and desorption on a $SrTiO_3$ photocatalyst excited under water†

Takumu Kosaka,[a] Tomohiro Ando,[b] Takashi Hisatomi,[cd] Hiroshi Nishiyama,[e] Yuanshu Zhou,[f] Kazunari Domen,[ce] Yasufumi Takahashi[df] and Hiroshi Onishi *[ag]

Received 17th July 2021,
Accepted 24th August 2021

DOI: 10.1039/d1cp03264j

rsc.li/pccp

Oxygen evolution at water–solid interfaces is a key reaction for sustainable energy production. Although some intermediate states have been detected in transient absorption spectroscopy, the O_2 evolution kinetics after the multi-step, four-electron oxidation of water remain unknown. In this study, transient amperometry with a microelectrode was applied to *operando* O_2 detection over Al-doped $SrTiO_3$ particles doubly loaded with $RhCrO_x$ and CoO_y cocatalysts, an efficient photocatalyst for the overall water-splitting reaction. Electrochemical O_2 detection at intervals of 0.1 s unexpectedly indicated instantaneous O_2 adsorption and desorption in addition to steady, photocatalytic O_2 evolution on the photocatalyst modified under intense light irradiation. We hypothesized that electrons excited in the conduction band were transferred to O_2 in water thorough Ti cations neighboring an oxygen anion vacancy on the modified Al-doped $SrTiO_3$. The negatively charged O_2 was then bound to the Ti cations. It was neutralized and released when shaded through electron back-transfer to the conduction band. The hypothesized mechanism for O_2 adsorption and desorption was compared with the photoinduced O_2 desorption known to occur on anion vacancies of TiO_2(110). The microelectrode-based transient amperometry demonstrated in this paper will be applied to many other phenomena at liquid–solid interfaces.

Introduction

Oxygen evolution at water–solid interfaces is a key reaction for sustainable energy production.[1–4] In semiconductor photocatalysts and photoelectrodes, the creation and consumption kinetics of bandgap-excited charge carriers[5–14] or chemical intermediates[15–20] have been traced using transient absorption spectroscopy (TAS) with good time resolutions of femtoseconds to milliseconds. The kinetics observed by TAS for the initial and intermediate species must be compared with O_2 evolution kinetics to verify or deny a proposed reaction mechanism. Nevertheless, it is still difficult to experimentally detect O_2 with a compatible time resolution.

Molecular oxygen released in water is currently accumulated in the gas phase and quantified with gas chromatography once or twice per hour. An improved time resolution on the scale of minutes could be achieved with advanced setups that shorten the gas-sampling intervals.[21] The authors have been developing a method using microelectrode-based transient amperometry to further speed up *operando* O_2 detection. Our simple idea is to shorten the physical distance from the place of reaction to the electrode for detection, as was conducted in scanning electrochemical microscopy (SECM) suitable for O_2 concentration mapping.[22–26] In our latest study,[27] we used diffusion simulations and electrochemical detection on a microelectrode to determine the absolute O_2 evolution rate with a time resolution of 0.1 s on a $SrTiO_3$ photocatalyst film immersed in a nitrogen-purged, aqueous KCl solution.

In the present study, the photocatalyst film was excited in an aerobic solution exposed to air. Surprisingly, molecular oxygen having been dissolved in the solution was adsorbed on the irradiated film, and it was released when shaded from the irradiation. We hypothesized that bandgap-excited electrons were injected into the O_2 in the solution. After receiving

[a] *Department of Chemistry, School of Science, Kobe University, Kobe 657-8501, Japan. E-mail: oni@kobe-u.ac.jp*
[b] *Division of Electrical Engineering and Computer Science, Kanazawa University, Kanazawa 920-1192, Japan*
[c] *Research Initiative for Supra-Materials, Interdisciplinary Cluster for Cutting Edge Research, Shinshu University, Nagano 380-8553, Japan*
[d] *Precursory Research for Embryonic Science and Technology, Japan Science and Technology Agency, Saitama 332-0012, Japan*
[e] *Office of University Professors, The University of Tokyo, Tokyo 113-8656, Japan*
[f] *Nano Life Science Institute, Kanazawa University, Kanazawa 920-1192, Japan*
[g] *Research Center for Membrane and Film Technology, Kobe University, Kobe 657-8501, Japan*

† Electronic supplementary information (ESI) available: Reagents, current responses, simulation details, X-ray photoelectron spectra, and optical absorption spectra. See DOI: 10.1039/d1cp03264j

the electrons, O_2 was negatively charged and bound to the Ti cations neighboring an oxygen anion vacancy on the surface of $SrTiO_3$.

Experimental section

The photocatalyst was $SrTiO_3$ particles doped with Al cations.[28] $SrTiO_3$, Al_2O_3, and $SrCl_2$ were mixed at a molar ratio of 100 : 2 : 10 and heated at 1423 K to produce Al-doped particles that were 200–500 nm in size. A $RhCrO_x$ cocatalyst (Rh 0.1 wt% and Cr 0.1 wt%) was loaded onto the particles using impregnation from an aqueous solution of Na_3RhCl_6 and $Cr(NO_3)_3$. A CoO_y cocatalyst (Co 0.1 wt%) was additionally loaded by photodeposition in an aqueous solution of $CoCl_2$. The $RhCrO_x$ cocatalyst was loaded for assisting electron-driven H_2 evolution,[29] whereas the CoO_y cocatalyst was for hole-driven O_2 evolution.[18,30] This photocatalyst was active for the overall water-splitting reaction with an apparent quantum yield of 55%. The photocatalyst particles were suspended in water with SiO_2 nanoparticles (1 : 2 weight ratio), dropped on a frosted glass plate, and dried at 323 K to be fixed. Photocatalyst-coated plates prepared in a similar manner had previously been placed in a panel reactor and tested for large-scale water splitting under natural sunlight.[28]

Details of the experimental setup are described in ref. 27 and its ESI. A millimeter-sized photocatalyst-coated glass plate was placed in a KCl aqueous solution (0.1 mol l^{-1}, pH = 7) that was exposed to air in this study. A platinum wire with a 10 μm radius was coated with glass to expose a metal section as the working electrode for O_2 detection. The electrode was immersed in the solution perpendicular to the photocatalyst film which was electrically isolated in the solution. The distance between the electrode and film was controlled in the 100–200 μm range with 0.1 μm precision. Molecular oxygen in the solution was electrochemically detected on the electrode with a time resolution of 0.1 s, which was biased at −0.5 V relative to a Ag wire as the counter electrode. A four-electron reduction reaction, $O_2 + 2H_2O + 4e^- \rightarrow 4OH^-$ and/or $O_2 + 4H^+ + 4e^- \rightarrow 2H_2O$,[31] produced an electrode current on the order of nano-amps that was proportional to the O_2 concentration. The proportional relation of O_2 concentration and electrode current was checked and confirmed.[27] The Ag wire served as a quasi Ag/AgCl reference electrode in the KCl solution. On the other hand, the oxidative reaction on the wire, $Ag + h^+ \rightarrow Ag^+$, as the counter electrode caused silver contamination in the solution to a limited extent. A freshly polished microelectrode was used in each set of measurements to minimize silver contamination on the microelectrode apex.

Results and discussion

The immersed film was side lit with ultraviolet (UV) light (center wavelength: 280 nm) passing through the solution, as illustrated in the table of contents entry. The light intensity was tuned to 3 W m^{-2} (4×10^{18} photons m^{-2} s^{-1}) to probe light-triggered O_2 concentration changes without producing O_2 and H_2 bubbles on the irradiated film. Fig. 1(A) presents the

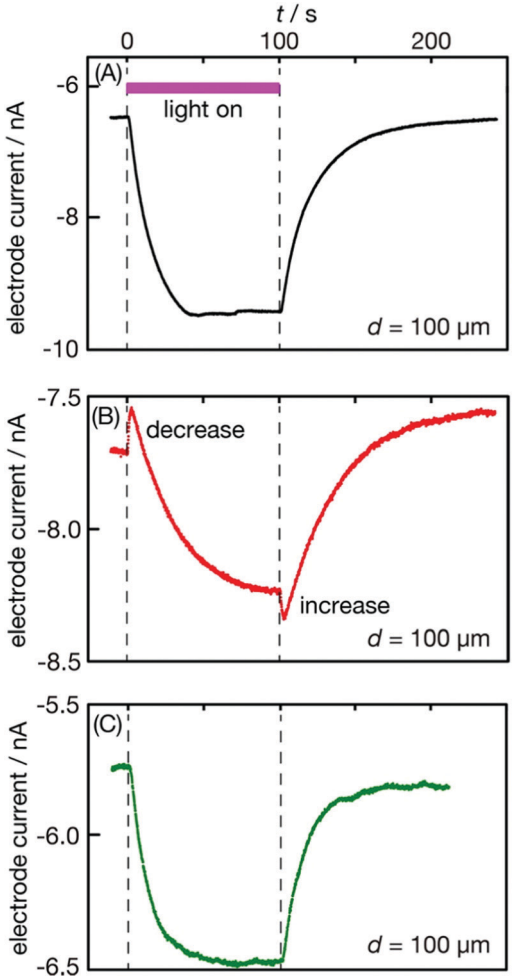

Fig. 1 Microelectrode current in response to UV light irradiation. Irradiation of a photocatalyst film with light for probing (intensity: 3 W m^{-2}) at t = 0–100.5 s in a KCl solution resulted in response (A). The film was then irradiated with intense light to modify the photocatalyst (30 W m^{-2}) for 4 h in the solution. Immediate irradiation of the modified film with light for probing (3 W m^{-2}) at t = 0–100.2 s resulted in response (B). The instantaneous current decrease and increase are marked in the panel. The film was removed from the solution and dried in air for 9 days. The dried film showed response (C) when immersed in the solution and irradiated with light for probing (3 W m^{-2}) at t = 0–101.1 s. The electrode–film distance d was set at 100 μm.

electrode current I that responded to light irradiation at an electrode–film distance d = 100 μm. The negative sign of the current indicates that electrons are transferred from the electrode to the solution. Molecular oxygen in the solution produced a background current of −6.5 nA. When the probe light was turned on at time zero (t = 0), the electrode current gradually increased to −9.5 nA; when the light stopped at 100.5 s, the current gradually decreased back to the background.

We had observed gradual current increases and decreases in response to UV light irradiation on the same photocatalyst,[27] where the whole setup was purged with N_2 to remove background O_2 in the solution. The current changes observed in the N_2 atmosphere were quantitatively interpreted with photocatalytic O_2 evolution on the irradiated film followed by O_2

diffusion into the bulk solution. The electrode current response shown in Fig. 1(A) increased and then decreased in a similar manner to what was reported in ref. 27 Hence, the response in Fig. 1(A) was ascribed to photocatalytic O_2 evolution on the irradiated film.

The film examined in Fig. 1(A) was then irradiated with UV light at 10 times the intensity (280 nm, 30 W m^{-2}) for 4 h in the solution. The film was photocatalytically active enough to produce O_2 and H_2 bubbles during this intense irradiation. The electrode current exceeded the quantification limit, 10.5 nA. When the intense irradiation was suspended, the film was immediately probed with weak light (3 W m^{-2}). Response (B) obtained in this way was qualitatively different from response (A). The electrode current was stable at −7.7 nA, indicating that O_2 was dissolved in the air-exposed solution prior to irradiation. When the probe light was switched on, the current instantaneously decreased from −7.7 to −7.5 nA. It then gradually increased, indicating photocatalytic O_2 production. When the probe light was stopped at t = 100.2 s, the electrode current instantaneously increased from −8.3 to −8.4 nA and gradually reduced back to the background level. We ascribed the instantaneous current increase coupled with the decrease to O_2 adsorption and desorption on the film triggered by light irradiation; background O_2 in the solution was adsorbed on the film when irradiated and was desorbed when shaded.

Pretreatment with intense light irradiation (30 W m^{-2} for 4 h) was required to modify the photocatalyst feasible for probe-light-triggered O_2 adsorption and desorption. Immersing the photocatalyst film in the solution for 4 h without intense light irradiation provided no instantaneous current response, as shown in Fig. S1 in the ESI.† Intense irradiation on the microelectrode induced no current response in the absence of the film (Fig. S2, ESI†). In a K_2SO_4 solution (0.1 mol l^{-1}), the film was modified under intense light to present similar instantaneous current responses (Fig. S3, ESI†) being insensitive to the chemical identity of electrolytes. Oxidation of Cl^- anions, if any on the UV-irradiated $SrTiO_3$ photocatalyst, did not matter to make the instantaneous current responses.

These experimental results supported our interpretation that probe-light-triggered O_2 adsorption and desorption occurred on the photocatalyst particles modified during the pretreatment.

After the film displayed response (B), it was removed from the solution and dried in air at room temperature for 9 days. This film was then immersed in the KCl solution and examined with probe light (3 W m^{-2}) again. The observed response (C) displayed a gradual current increase and decrease, which were attributed to photocatalytic O_2 evolution; no instantaneous response could be assigned to O_2 adsorption and desorption. The modified photocatalyst particles returned to their original state when dried in air.

In the descriptions above, we qualitatively characterized the electrode current responses according to the presence or absence of instantaneous responses triggered by probe-light irradiation. We then quantitatively interpreted response (B) in Fig. 1, using a numerical simulation including instantaneous O_2 adsorption, photocatalytic O_2 evolution, instantaneous O_2 desorption, and O_2 diffusion in the solution. The simulation space defined in cylindrical coordinates, r and z, is illustrated in Fig. 2(A). The oxygen diffusion driven by a concentration gradient is described by Fick's law:

$$\frac{\partial C}{\partial t} = D\left(\frac{\partial^2 C}{\partial r^2} + \frac{1}{r}\frac{\partial C}{\partial r} + \frac{\partial^2 C}{\partial z^2}\right)$$

where C is concentration, and D is the diffusion coefficient of O_2 ($D = 2.5 \times 10^{-5}$ cm^2 s^{-1} at 298 K).[32] The details of the finite-element scheme, which integrates the equation to predict the electrode current, are described with Fig. S4 in ESI.† To fit the experimentally observed response shown in Fig. 1(B), we assumed probe-light-triggered O_2 adsorption at $t = 0 - \tau$, photocatalytic O_2 evolution at $t = \tau - 100.2$ s, and O_2 desorption at $t = 100.2$ s $-$ (100.2 s + τ), as depicted in Fig. 2(B). Positive and negative O_2 release rates in the unit of μmol m^{-2} s^{-1} were used to represent O_2 release and suction on the film, respectively. The time width τ was not necessarily identical for the adsorption and desorption phenomena. However, a common τ value was assumed to minimize the number of fitting parameters.

The O_2 release rate depicted in Fig. 2(B) represented a net release rate. When light-triggered O_2 absorption or desorption occurred with photocatalytic O_2 evolution in parallel, the net release rate was evaluated by fitting simulated current responses to the experimental result.

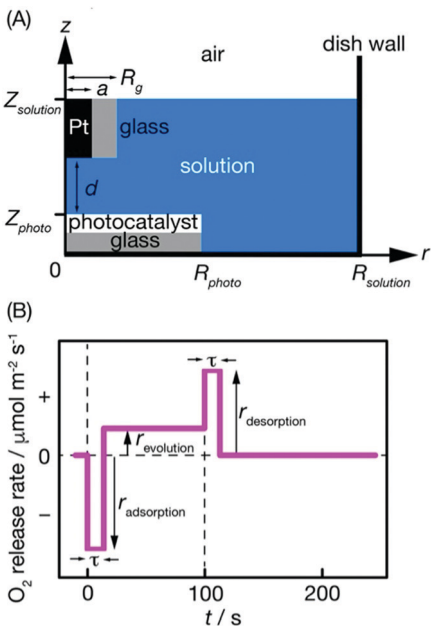

Fig. 2 Finite-element simulation of electrode current. The simulation space, which has cylindrical symmetry around the z-axis, is illustrated in (A). Platinum electrode section radius, a: 10 μm; glass wrap outer radius, R_g: 20 μm; electrode–film distance, d: 100 μm; radius of the irradiated photocatalyst film, R_{photo}: fitted to be 800 μm in the simulation (see text); solution dish radius, $R_{solution}$: 13 mm; solution thickness, $Z_{solution}$: 10 mm; glass plate thickness, Z_{photo}: 1 mm. The solid line in (B) depicts the assumed O_2 release rate on the film.

The simulated current was fitted to the experimental result in two steps. In the first step, R_{photo} and $r_{evolution}$ were optimized to follow the gradual current increase during probe-light irradiation, while τ was set to zero. The other quantities (a, R_g, d, $R_{solution}$, $Z_{solution}$, and Z_{photo}) were fixed at experimentally determined values, as described in the caption of Fig. 2. The radius of the irradiated photocatalyst film R_{photo} was difficult to quantitatively determine since the light-spot boundary was oval and graded on the film. Thus, R_{photo} and $r_{evolution}$ were optimized to fit the experimentally observed response. The obtained R_{photo} was 800 μm, while $r_{evolution}$ was 0.085 μmol m^{-2} s^{-1}. In the second step, $r_{adsorption}$ and τ were fitted to the observed response for t = 0–10 s. Fitting to the response in t = 0–10 s was long enough to evaluate the impulsive O_2 suction having occurred at $t = 0 - \tau$, since the time delay for diffusion across the electrode–film gap was characterized by d^2/D = 4 s.

When irradiation was stopped, $r_{desorption}$ and τ were optimized to follow the observed response at t = 100–110 s. The current response simulated in this way was compared with the observed response in Fig. 3, in which the background current (−7.7 nA) was subtracted to deduce the current change induced by probe-light irradiation. The simulated response reproduced the observed current in the three time windows, t = 0–250, 0–10, and 95–110 s, and the optimized parameters were $r_{adsorption}$ = −0.35 μmol m^{-2} s^{-1}, $r_{desorption}$ = 0.21 μmol m^{-2} s^{-1}, and τ = 2.0 s. Two more response curves were experimentally observed on the same film upon changing d to 150 and 200 μm (Fig. 4). The two curves were fitted to validate the simulation scheme and the optimized parameters.

A negative release rate of −0.35 μmol m^{-2} s^{-1} was evaluated in the first 2.0 s of probe-light irradiation. The integrated quantity of adsorbed O_2, which was calculated as the product of $r_{adsorption}$ and τ, had a value of 4.2×10^{17} molecules m^{-2}. The integrated quantity corresponded to 6% of the surface unit cell density of crystalline $SrTiO_3$, 6.6×10^{18} m^{-2} on its (100) truncation.[33] The integrated quantity suggests O_2 adsorption on $SrTiO_3$ rather than on the $RhCrO_x$ and/or CoO_y cocatalysts loaded by 0.1 wt%. Partial contribution of the cocatalysts cannot be excluded, though. Since the film was composed of particulate materials, the unit cell density exposed to the solution should be larger than this number. Hence, the integrated quantity of 6% relative to the unit cell density provides the maximum estimate.

The integrated quantity of desorbed O_2, which was calculated as the product of $r_{desorption}$ and τ, had a value of 2.5×10^{17} molecules m^{-2}. The desorbed quantity was 40% smaller than the adsorbed quantity. The decremental difference was ascribed to O_2 desorption during probe-light irradiation or to the conversion of the adsorbed O_2 to resident species on the shaded film.

Finally, we considered the mechanism through which O_2 in the solution was adsorbed on the Al-doped $SrTiO_3$ particles. Several peroxotitanate complexes having Ti metal centers coordinated by O_2^{2-} ligands were previously reported.[34] We therefore hypothesize that negatively charged O_2 species, possibly O_2^{2-}, were bound to Ti cations on the surface of the $SrTiO_3$ during probe-light irradiation. Bandgap excitation by probe light provided two electrons, which were transferred to an impinging O_2 molecule. By shading the particles, the electrons were back-transferred to the photocatalyst particle, resulting in the release of the neutralized O_2 into the solution.

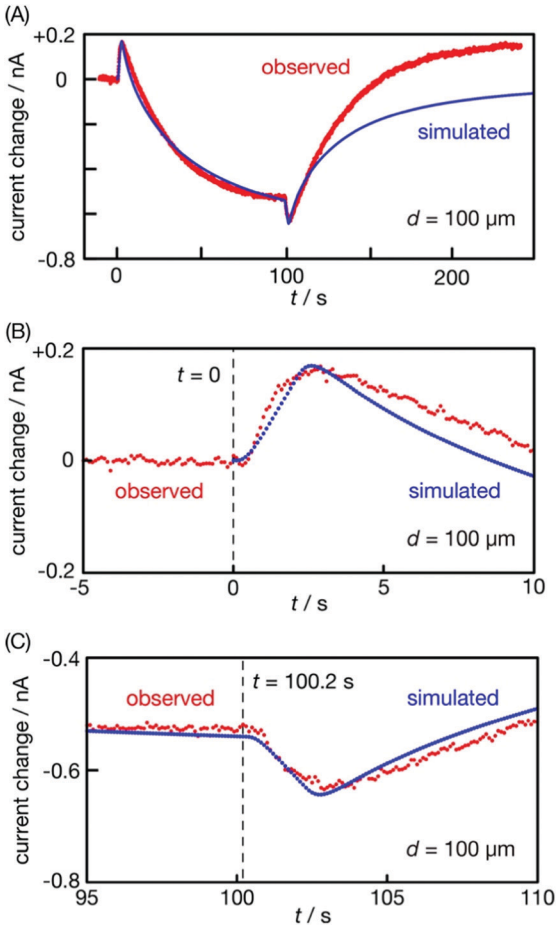

Fig. 3 Electrode current response shown in Fig. 1(B) fitted with the finite-element simulation of O_2 adsorption, evolution, and desorption on the photocatalyst film. The experimentally observed (red) and simulated (blue) current changes are shown in time windows of (A) 0–250, (B) 0–10, and (C) 95–110 s. Electrode–film distance d = 100 μm. UV light (3 W m^{-2}) was irradiated for probing on the photocatalyst film at t = 0–100.2 s. Five fitting parameters were optimized: R_{photo} = 800 μm, $r_{evolution}$ = 0.085 μmol m^{-2} s^{-1}, $r_{adsorption}$ = −0.35 μmol m^{-2} s^{-1}, $r_{desorption}$ = 0.21 μmol m^{-2} s^{-1}, and τ = 2.0 s.

Titanium cations exposed on pristine particles were unable to capture O_2 even under the probe light, as was evidenced by the absence of the instantaneous current response in Fig. 1(A). The surface of the particles was modified during the pretreatment under intense light irradiation (30 W m^{-2}) to enable the capture of negatively charged O_2. The modified surface returned to its original state when the film was dried in air at room temperature. The reversible state changes suggested that a limited number of oxygen anions were removed during the pretreatment and resultant anion vacancies served as active site for O_2 adsorption. The vacancies were healed on the dried film. If metal (Sr, Ti, Al, Cr, Rh or Co) cations were removed under irradiation and induced the light-triggered adsorption, then they could not be restored when the surface was dried in air.

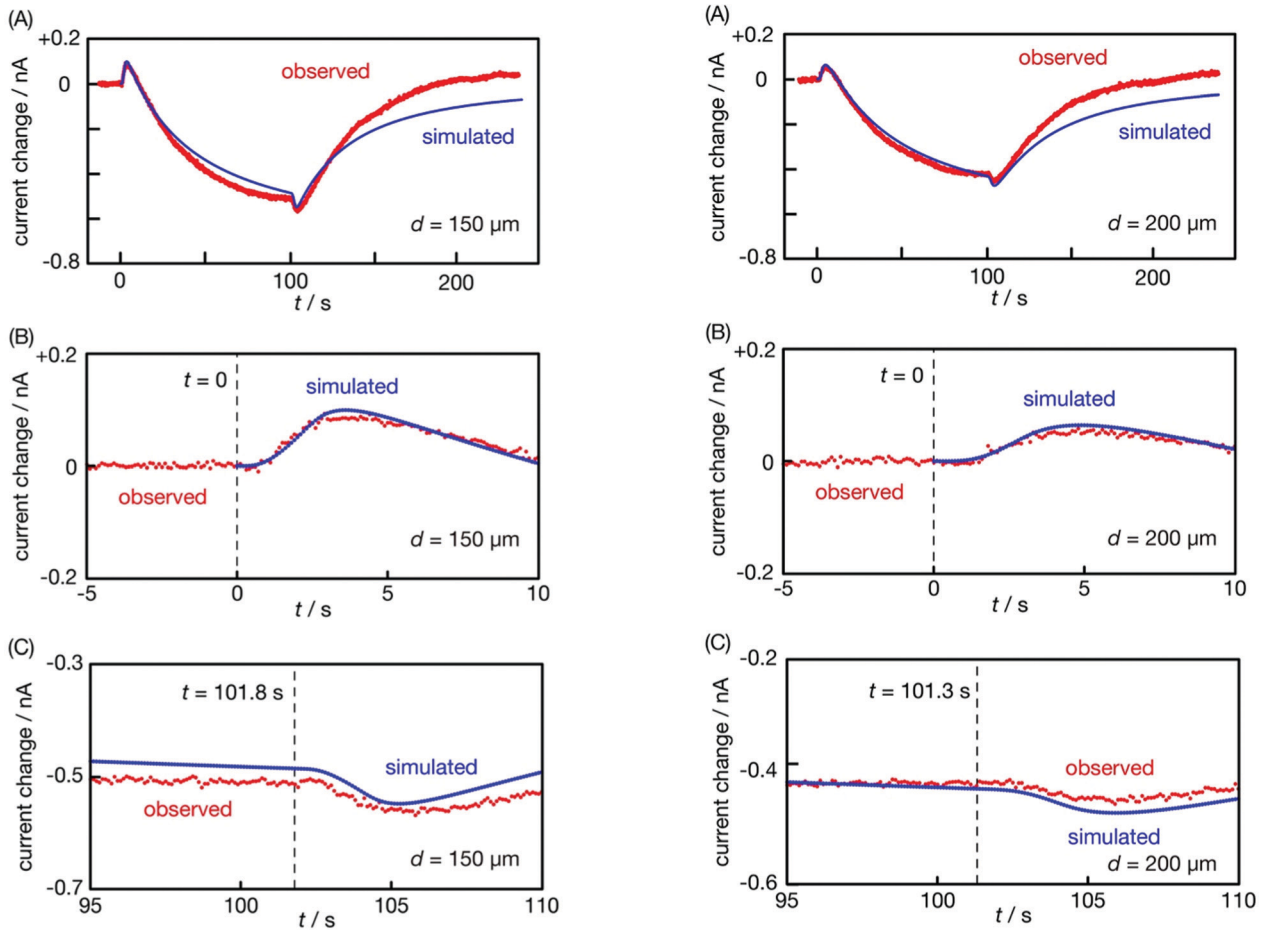

Fig. 4 Current changes at d = (left panel) 150 and (right panel) 200 μm. The experimentally observed (red) and simulated (blue) current changes are shown in time windows of (A) 0–250, (B) 0–10, and (C) 95–110 s. UV light for probing (3 W m^{-2}) was irradiated on the film at t = (left panel) 0–101.8 and (right panel) t = 0–101.3 s. The five fitting parameters (R_{photo}, $r_{evolution}$, $r_{adsorption}$, $r_{desorption}$, and τ) were fixed at values optimized in the simulation at d = 100 μm.

An analogous mechanism for O_2 adsorption and desorption is known to occur on TiO_2(110) wafers placed in vacuum. Experimental[35,36] and theoretical[37] studies have concluded that O_2 was adsorbed on Ti^{3+} cations that neighbored an oxygen anion vacancy when the vacancy was thermally created on the wafer surface. The adsorbed O_2 receives two excess electrons that were originally localized on the Ti^{3+} cations. When the wafer is bandgap excited, two holes attached to the negatively charged O_2 and the neutralized O_2 escaped as gas. Electron transfer and back-transfer switched the O_2 adsorption and desorption on the anion vacancy.

We further hypothesized how oxygen anions were removed from Al-doped $SrTiO_3$ particles during the pretreatment. Upon capture of two holes, an oxygen anion is neutralized and leave the surface. This process is known as photocorrosion;[38] however, $SrTiO_3$ is recognized as a stable semiconductor against photocorrosion. The neutralization of an oxygen anion leading to vacancy creation thermodynamically and kinetically competes with water oxidation, when a metal oxide particle is excited under water. The electrochemical potential for this phenomenon, *i.e.*, corrosion potential, is known to be 1.42 eV *vs.* NHE on TiO_2 in water having a pH of 0. On the other hand, the potential for water oxidation is 1.23 eV at pH 0. When we assume an identical corrosion potential on the surface of Al-doped $SrTiO_3$, photoexcited holes are thermodynamically transferred to water and not to surface oxygen anions.

A finite number of holes are still feasible for neutralizing oxygen anions when water oxidation is kinetically limited. The Al-doped $SrTiO_3$ photocatalyst examined in this study was doubly loaded with the $CrRhO_x$ cocatalyst for electron-driven H_2 production[29] and the CoO_y cocatalyst for hole-driven O_2 production.[28] A finite number of holes could have been present in Al-doped $SrTiO_3$ particles even modified with the CoO_y cocatalyst for water oxidation.

Thus, the authors hypothesized that a small number of oxygen anions were neutralized and removed during the pretreatment under intense light irradiation. Indeed, a previous study[39] reported photoetching of TiO_2 electrodes which is known to be thermodynamically stable oxide against photocorrosion. The self-oxidation of the cocatalysts, if any during the pretreatment, may have created oxygen vacancies on the cocatalysts and contributed to the probe-light induced O_2 adsorption and desorption.

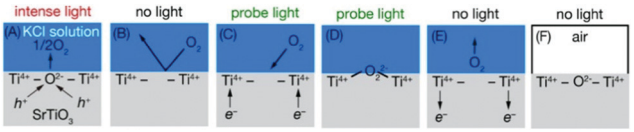

Fig. 5 A possible mechanism for light-triggered O_2 adsorption on the Al-doped $SrTiO_3$ photocatalyst particles. (A) A surface oxygen anion neutralized and removed during intense light irradiation (30 W m^{-2}). (B) No O_2 adsorption to the vacancy in the electronic ground state. (C) O_2 adsorption to the vacancy, assisted by electrons excited under probe-light irradiation (3 W m^{-2}). (D) Adsorption of a negatively charged O_2 on the vacancy. (E) O_2 desorption under shaded conditions, with electrons leaving. (F) The anion vacancy slowly healed in air at room temperature.

The hypothesized mechanism is depicted in Fig. 5. In panel (A), a small number (6% or less relative to surface lattice density) of surface oxygen anions of Al-doped $SrTiO_3$ are neutralized and removed during the pretreatment. The large number of holes excited under intense light irradiation drive this step. Excited electrons corresponding to the holes that neutralize the anions are consumed in the H_2 evolution reaction, $2H_2O + 2e^- \rightarrow H_2 + 2OH^-$. The OH anions left in the reaction can be released in the solution. The ionic charges in the particle are balanced without need of creating Ti^{3+} cations, as a result. (B) O_2 cannot be adsorbed on the anion vacancy when shaded. (C) Under probe-light irradiation, electrons excited in the particle are transferred to an impinging O_2 through Ti cations neighboring the vacancy. (D) The negatively charged O_2 is bound to the vacancy. (E) When the probe light is turned off, the excited electrons leave the adsorbed O_2, and the neutralized O_2 is released into the solution. The electrons leaving the adsorbed O_2 are consumed in the H_2 evolution reaction. (F) The anion vacancies were slowly healed after the film was dried in air.

O_2 desorption leaving an oxygen anion vacancy, which was hypothesized in Fig. 5(E), is identical to the O_2 release step in the lattice oxygen evolution reaction (LOER), *e.g.*, Fig. 4 of ref. 3 LOER has been recently proposed as an electrochemical cycle of the O_2 evolution reaction on perovskite-structured metal oxide electrodes; it is different from the proton-coupled electron transfer[4] that was previously assumed as the mechanism.

To investigate our hypothesis, we compared the photocatalyst films before and after the pretreatment using X-ray photoelectron spectroscopy (Fig. S5, ESI†) and optical absorption (Fig. S6, ESI†). The results show no sign of reduced Ti cations. This is consistent with the proposed scheme (Fig. 5), which involves Ti cations only in the 4+ valence state.

The $SrTiO_3$ particles were doped with Al cations in this study to enhance water-splitting efficiency by limiting electron–hole recombination. Transient absorption studies[40,41] showed recombination rate in $SrTiO_3$ particles decreased by Na doping, whereas recombination rate was not yet examined on Al-doped $SrTiO_3$. It is possible that the Al cations embedded in $SrTiO_3$ lattice played a positive or negative role in removing oxygen anions and in the instantaneous O_2 responses. This possibility should be examined in the future.

The light-triggered O_2 adsorption and desorption found in this study open an additional path for electron–hole recombination. Two excited electrons can be located in an O_2 adsorbed on the vacancy. These electrons recombine with two holes, thus releasing the adsorbed O_2 under steady light irradiation. Two electrons and holes are consumed to catch and release an O_2 molecule in the solution without splitting water.

In addition, the hypothesized hole-induced vacancy creation is a side-reaction that is problematic for photocatalyst durability. Durability of the Al-doped $SrTiO_3$ photocatalyst was enhanced over a span of 1300 h under simulated sunlight irradiation by loading the CoO_y cocatalyst.[30] The limited durability in the absence of CoO_y was interpreted with hole-induced degradation of the $RhCrO_x$ cocatalyst. The hole-induced vacancy creation hypothesized in this study may have been an additional reason of the limited durability.

A semiconductor photocatalyst that efficiently drives the water-splitting reaction is potentially modified by the hole-induced creation of anion vacancies since electron–hole recombination is limited to increased quantum yields. Note that the light intensity for vacancy creation was 30 W m^{-2} near UV intensity in natural sun light (40 W m^{-2} for wavelengths shorter than 400 nm). When this occurs on a photocatalyst under development, the tuning of cocatalysts to accelerate water-induced, hole-consuming reactions can be a beneficial way to optimize the number of holes present in the semiconductor particles under excitation light of a given intensity.

Conclusion

In this study, we found that the O_2 adsorption and desorption on the Al-doped $SrTiO_3$ photocatalyst particles doubly loaded with $RhCrO_x$ and CoO_y cocatalysts were triggered by photoexcitation in water. Electrochemical detection on the microelectrode combined with diffusion simulations allowed us to quantitatively determine the rates of O_2 adsorption, O_2 desorption, and photocatalytic O_2 evolution. The time resolution for O_2 detection, 0.1 s, was critical for recognizing the instantaneous O_2 adsorption and desorption that occurred during steady O_2 evolution. The transient amperometry using a microelectrode can be applied to many other phenomena at liquid–solid interfaces.

The light-triggered O_2 adsorption and desorption were interpreted as the excited-electron transfer to and back-transfer from the adsorbed O_2. Upon receiving electrons, O_2 in the solution was negatively charged and could bind to the surface Ti^{4+} cations, while shaded particles could neutralize and release O_2 by back-transferring the electrons. Intense light irradiation (30 W m^{-2}) was required to modify the particle to enable O_2 adsorption. We hypothesized that a small number of lattice oxygen anions were neutralized by receiving holes to leave the surface under intense irradiation. Anion vacancies created in this way served as O_2 adsorption sites. Future studies that examine the role of the Al cations, $RhCrO_x$ cocatalyst, and CoO_y cocatalyst are needed to verify the hypothesized scheme.

Conflicts of interest

There are no conflicts to declare.

Acknowledgements

Yasuko Kuromiya, Yoshie Nagatuma, and Masaharu Yamaguchi are thanked for their technical assistance. This work was supported by JSPS KAKENHI (grant numbers: JP19H00915 and 18KK0161). T. H. and Y. T. acknowledge support from PRESTO (JPMJPR20T9 and JPMJPR18T8) respectively from the Japan Science and Technology Agency.

References

1 H. Inoue, T. Shimada, Y. Kou, Y. Napitane, D. Masui, S. Takagi and H. Tachibana, The Water Oxidation Bottleneck in Artificial Photosynthesis: How can We Get Through It? An Alternative Route Involving a Two-electron Process, *ChemSusChem*, 2011, **4**, 173–179.

2 F. Song, L. Bai, A. Moysiadou, S. Lee, C. Hu, L. Liardet and X. Hu, Transition Metal Oxides as Electrocatalysts for the Oxygen Evolution Reaction in Alkaline Solutions: An Application-inspired Renaissance, *J. Am. Soc. Chem.*, 2018, **140**, 7748–7759.

3 E. Fabbri and T. J. Schmidt, Oxygen Evolution Reaction—The Enigma in Water Electrolysis, *ACS Catal.*, 2018, **8**, 9765–9774.

4 J. Rossmeisl, Z.-W. Qu, H. Zhu, G.-J. Kroes and J. K. Nørskov, Electrolysis of Water on Oxide Surfaces, *J. Electroanal. Chem.*, 2007, **607**, 83–89.

5 C. Kranz and M. Wächtler, Characterizing photocatalysts for water splitting: from atoms to bulk and from slow to ultrafast processes, *Chem. Soc. Rev.*, 2021, **50**, 1407–1437.

6 Y. Paz, Transient IR spectroscopy as a tool for studying photocatalytic materials, *J. Phys.: Condens. Matter*, 2019, **31**, 503004.

7 K. Takanabe, Photocatalytic Water Splitting: Quantitative Approaches toward Photocatalyst by Design, *ACS Catal.*, 2017, **7**, 8006–8022.

8 A. Yamakata, T. Ishibashi and H. Onishi, Kinetics of the Photocatalytic Water-Splitting Reaction on TiO_2 and Pt/TiO_2 Studied by Time-Resolved Infrared Absorption Spectroscopy, *J. Mol. Catal. A: Chem.*, 2003, **199**, 85–94.

9 T. Yoshihara, R. Katoh, A. Furube, Y. Tamaki, M. Murai, K. Hara, S. Murata, H. Arakawa and M. Tachiya, Identification of Reactive Species in Photoexcited Nanocrystalline TiO_2 Films by Wide-Wavelength-Range (400–2500 nm) Transient Absorption Spectroscopy, *J. Phys. Chem. B*, 2004, **108**, 3817–3823.

10 J. Tang, J. R. Durrant and D. R. Klug, Mechanism of Photocatalytic Water Splitting in TiO_2. Reaction of Water with Photoholes, Importance of Charge Carrier Dynamics, and Evidence for Four-Hole Chemistry, *J. Am. Chem. Soc.*, 2008, **130**, 13885–13891.

11 M. Maruyama, A. Iwase, H. Kato, A. Kudo and H. Onishi, Time-Resolved Infrared Absorption Study of $NaTaO_3$ Photocatalysts Doped with Alkali Earth Metals, *J. Phys. Chem. C*, 2009, **113**, 13918–13923.

12 Y. Ma, S. R. Pendlebury, A. Reynal, F. Le Formal and J. R. Durrant, Dynamics of photogenerated holes in undoped $BiVO_4$ photoanodes for solar water oxidation, *Chem. Sci.*, 2014, **5**, 2964–2973.

13 F. Le Formal, E. Pastor, S. D. Tilley, C. A. Mesa, S. R. Pendlebury, M. Grätzel and J. R. Durrant, Rate Law Analysis of Water Oxidation on a Hematite Surface, *J. Am. Chem. Soc.*, 2015, **137**, 6629–6637.

14 T. J. Miao and J. Tang, Characterization of charge carrier behavior in photocatalysis using transient absorption spectroscopy, *J. Chem. Phys.*, 2020, **152**, 194201.

15 Y. Nosaka and A. Y. Nosaka, Generation and Detection of Reactive Oxygen Species in Photocatalysis, *Chem. Rev.*, 2017, **117**, 11302–11336.

16 R. Nakamura and Y. Nakato, Primary Intermediates of Oxygen Photoevolution Reaction on TiO_2 (Rutile) Particles, Revealed by in Situ FTIR Absorption and Photoluminescence Measurements, *J. Am. Chem. Soc.*, 2004, **126**, 1290–1298.

17 N. Sivasankar, W. W. Weare and H. Frei, Direct Observation of a Hydroperoxide Surface Intermediate upon Visible Light-Driven Water Oxidation at an Ir Oxide Nanocluster Catalyst by Rapid-Scan FT-IR Spectroscopy, *J. Am. Chem. Soc.*, 2011, **133**, 12976–12979.

18 M. Zhang, M. de Respinis and H. Frei, Time-resolved observations of water oxidation intermediates on a cobalt oxide nanoparticle catalyst, *Nat. Chem.*, 2014, **6**, 362–367.

19 D. M. Herlihy, M. M. Waegele, X. Chen, C. D. Pemmaraju, D. Prendergast and T. Cuk, Detecting the oxyl radical of photocatalytic water oxidation at an n-$SrTiO_3$/aqueous interface through its subsurface vibration, *Nat. Chem.*, 2016, **8**, 549–555.

20 O. Zandi and T. W. Hamann, Determination of photoelectrochemical water oxidation intermediates on haematite electrode surfaces using *operando* infrared spectroscopy, *Nat. Chem.*, 2016, **8**, 778–783.

21 K. Han, T. Kreuger, B. Mei and G. Mul, Transient behavior of $Ni@NiO_x$ functionalized $SrTiO_3$ in overall water splitting, *ACS Catal.*, 2017, **7**, 1610–1614.

22 J. Lee, H. Ye, S. Pan and A. J. Bard, Screening of Photocatalysts by Scanning Electrochemical Microscopy, *Anal. Chem.*, 2008, **80**, 7445–7450.

23 M. Plaza, X. Huang, J. Y. P. Ko, M. Shen, B. H. Simpson, J. Rodríguez-López, N. L. Ritzert, K. Letchworth-Weaver, D. Gunceler, D. G. Schlom, T. A. Arias, J. D. Block and H. D. Abruña, Structure of the Photo-catalytically Active Surface of $SrTiO_3$, *J. Am. Chem. Soc.*, 2016, **138**, 7816–7819.

24 J. H. Bae, A. B. Nepomnyashchii, X. Wang, D. V. Potapenko and M. V. Mirkin, Photo-scanning Electrochemical Microscopy on the Nanoscale with Through-tip Illumination, *Anal. Chem.*, 2019, **91**, 12601–12605.

25 X. Zhou, Z. T. Gossege, B. H. Simpson, J. Hui, Z. J. Barton and J. Rodríguez-López, Electrochemical Imaging of Photoanodic Water Oxidation Enhancements on TiO_2 Thin Films Modified by Subsurface Aluminum Nanodimers, *ACS Nano*, 2016, **10**, 9346–9352.

26 K. Ikeda, H. Sakai, R. Baba, K. Hashimoto and A. Fujishima, Photocatalytic Reactions Involving Radical Chain Reactions Using Microelectrodes, *J. Phys. Chem. B*, 1997, **101**, 2617–2620.

27 T. Kosaka, Y. Teduka, T. Ogura, Y. Zhou, T. Hisatomi, H. Nishiyama, K. Domen, Y. Takahashi and H. Onishi, Transient Kinetics of O_2 Evolution in Photocatalytic Water-Splitting Reaction, *ACS Catal.*, 2020, **10**, 13159–13164.

28 Y. Goto, T. Hisatomi, Q. Wang, T. Higashi, K. Ishikiriyama, T. Maeda, Y. Sakata, S. Okunaka, H. Tokudome, M. Katayama, S. Akiyama, H. Nishiyama, Y. Inoue, T. Takewaki, T. Setoyama, T. Minegishi, T. Takata, T. Yamada and K. Domen, A particulate photocatalyst water-splitting panel for large-scale solar hydrogen generation, *Joule*, 2018, **2**, 509–520.

29 M. Yoshida, K. Takanabe, K. Maeda, A. Ishikawa, J. Kubota, Y. Sakata, Y. Ikezawa and K. Domen, Role and Function of Noble-Metal/Cr-Layer Core/Shell Structure Cocatalysts for Photocatalytic Overall Water Splitting Studied by Model Electrodes, *J. Phys. Chem. C*, 2009, **113**, 10151–10157.

30 H. Lyu, T. Hisatomi, Y. Goto, M. Yoshida, T. Higashi, M. Katayama, T. Takata, T. Minegishi, H. Nishiyama, T. Yamada, Y. Sakata, K. Asakura and K. Domen, An Al-doped $SrTiO_3$ photocatalyst maintaining sunlight-driven overall water splitting activity for over 1000 h of constant illumination, *Chem. Sci.*, 2019, **10**, 3196–3201.

31 E. Yeager, Electrocatalysts for O_2 reduction, *Electrochim. Acta*, 1984, **29**, 1527–1537.

32 *Handbook of Chemistry: Pure Chemistry*, Chemical Society of Japan, Maruzen, Tokyo, 4th edn, 1993, p. II-63.

33 The surface unit cell density was calculated with the cubic unit cell length (0.390 nm) reported in Y. A. Abramov, V. G. Tsirelson, V. E. Zavodnik, S. A. Ivanov and I. D. Brown, The Chemical Bond and Atomic Displacements in $SrTiO_3$ from X-ray Diffraction Analysis, *Acta Crystallogr., Sect. B: Struct. Sci.*, 1995, **51**, 942–951.

34 M. Kakihana, M. Tada, M. Shiro, V. Petrykin, M. Osada and Y. Nakamura, Structure and Stability of Water Soluble $(NH_4)_8[Ti_4(C_6H_4O_7)_4(O_2)_4]\cdot 8H_2O$, *Inorg. Chem.*, 2001, **40**, 891–894 and references therein.

35 G. Lu, A. Linsebigler and J. T. Yates, Jr., The photochemical identification of two chemisorption states for molecular oxygen on $TiO_2(110)$, *J. Chem. Phys.*, 1995, **102**, 3005–3008.

36 N. G. Petrik and G. A. Kimmel, Electron- and Hole-Mediated Reactions in UV-Irradiated O_2 Adsorbed on Reduced Rutile $TiO_2(110)$, *J. Phys. Chem. C*, 2011, **115**, 152–164.

37 M. P. de Lara-Castells and J. L. Krause, Theoretical study of the UV-induced desorption of molecular oxygen from the reduced $TiO_2(110)$ surface, *J. Chem. Phys.*, 2003, **118**, 5098–5105.

38 H. Gerischer, Solar Photoelectrolysis with Semiconductor Electrodes, in *Solar Energy Conversion, Solid-State Physics Aspects*, ed. B. O. Seraphin, Springer-Verlag, Berlin, 1979, p. 141.

39 A. Tsujiko, T. Kisumi, Y. Magari, K. Kurakoshi and Y. Nakatao, Selective Formation of Nanoholes with (100)-Face Walls by Photoetching of *n*-TiO_2 (Rutile) Electrodes, Accompanied by Increases in Water-Oxidation Photocurrent, *J. Phys. Chem. B*, 2000, **104**, 4873–4879.

40 K. Kato, J. Jiang, Y. Sakata and A. Yamakata, Effect of Na-Doping on Electron Decay Kinetics in $SrTiO_3$ Photocatalyst, *ChemCatChem*, 2019, **11**, 6349–6354.

41 J. Jiang, K. Kato, H. Fujimori, A. Yamakata and Y. Sakata, Investigation on the highly active $SrTiO_3$ photocatalyst toward overall H_2O splitting by doping Na ion, *J. Catal.*, 2020, **390**, 81–89.